Research Article

Columbite-group minerals and mica of peraluminous granite record the magmatic-hydrothermal processes that formed the Zhaojinggou Ta—Nb deposit in the North China Craton

Bo Wei [a,b,*], Christina Yan Wang [a,b], Zhenhua Zhao [a], Hongtian Bao [a,c]

[a] Key Laboratory of Mineralogy and Metallogeny, Guangzhou Institute of Geochemistry, Chinese Academy of Sciences, Guangzhou 510640, China
[b] Guangdong Provincial Key Laboratory of Mineral Physics and Materials, Guangzhou 510640, China
[c] University of Chinese Academy of Sciences, Beijing 100049, China

ARTICLE INFO

ABSTRACT

The newly discovered Zhaojinggou Ta—Nb deposit in the northern margin of the North China Craton contains ore reserves of more than 38 Mt. at an average grade of 0.013 wt% Ta_2O_5 and 0.012 wt% Nb_2O_5. The Ta—Nb mineralization is mainly hosted in a peraluminous, albite granite body, which is about 400 m long and 20 to 100 m wide, with a surface exposure of ~0.05 km^2. Granitic pegmatites and greisen veins that range from several centimeters to meters in width, occur in the margin of the granite body, and wolframite-quartz veins intrude the wall rocks up to tens of meters away from the granite contact. LA-ICP-MS U—Pb dating for columbite of the granite yields the lower intercept ages between 131.8 ± 1.0 Ma and 134.6 ± 2.1 Ma on the Tera-Wasserburg concordia diagram, indicating that the mineralization occurred in the early Cretaceous, coeval with the peak stage of lithospheric thinning and destruction of the North China Craton. The columbite grains in the granite are commonly euhedral, and are surrounded or penetrated by irregular tantalite patches/rims containing Ta_2O_5 as high as 59.5 wt%. The Ta concentrations within single columbite crystals commonly increase slightly from the center outwards, consistent with a systematic decrease of Nb/Ta caused by crystallization of columbite from the silicic magma. Mica in the granite shows disordered bright and dark domains in their BSE images; bright domains are F-rich zinnwaldite crystallized from highly evolved melts that were relatively enriched in Fe, Li, Rb, Nb and Ta, whereas the dark domains are F-poor muscovite crystallized from later hydrothermal fluids that were relatively enriched in Al, Mn, Ba, Sn and W. It is thus likely that the tantalite patches/rims around the columbite grains crystallized from a Ta- and F-rich hydrosilicate melt in a magmatic-hydrothermal transitional stage. The wolframite-quartz veins adjacent to the granite body likely formed from a W-rich hydrothermal fluid.

© 2020 Elsevier B.V. All rights reserved.

1. Introduction

Tantalum and Nb are critical metals in the high-tech electronics industry. Global Ta resources are mainly produced from LCT-type (Li, Cs- and Ta-enriched), peraluminous pegmatites and granites (Linnen and Cuney, 2005). Although most of the Ta mined thus far is from LCT-type pegmatites, such as those of the Tanco deposit of Canada (Van Lichtervelde) and the Greenbushes deposit of Australia (Partington et al., 1995), peraluminous granites can also contain significant reserves of Ta, such as the Yichun granite in China (Huang et al., 2002), the Orlovka granite in Russia (Reyf et al., 2000), and the Nuweibi granite in Egypt (Helba et al., 1997).

Most Ta- and Nb-bearing minerals in peraluminous granites belong to the columbite group (Linnen et al., 2014 and references therein), but it is still not clear how the Ta-rich phases form. Experimental results show that Ta has a higher affinity for silicate melts than for hydrothermal fluids (Linnen and Cuney, 2005; Linnen and Keppler, 1997), but textural relationships and compositions of columbite-group minerals suggest derivation from late exsolved, hydrothermal fluids or fluid-rich melts (Anderson et al., 2013; Dostal et al., 2015; Neiva et al., 2015; Rao et al., 2009; Wu et al., 2018; Zhu et al., 2015). Columbite-group minerals in peraluminous granites usually exhibit complex zoning patterns of Nb, Ta and other trace elements (Alfonso et al., 2018; Tindle and Breaks, 2000; Wang et al., 1997), reflecting the evolution of the host granite. In addition, mica is common in peraluminous granites where include both magmatic and hydrothermal varieties (Li et al., 2015; Kaeter et al., 2018; Breiter et al., 2019), thus providing diagnostic information on the magmatic-hydrothermal processes of the granitic magmas.

* Corresponding author at: Key Laboratory of Mineralogy and Metallogeny, Guangzhou Institute of Geochemistry, Chinese Academy of Sciences, Guangzhou 510640, China.
E-mail address: weibo@gig.ac.cn (B. Wei).

The Zhaojinggou Ta—Nb deposit in the North China Craton contains ore reserves of more than 38 Mt. with an average grade of 0.013 wt% Ta_2O_5 and 0.012 wt% Nb_2O_5 (Chai and Wu, 2013). The Ta—Nb mineralization is hosted in a peraluminous, albite granite body. The columbite-group minerals and micas in the granite display diverse zoning patterns in BSE images, and we use this information to decipher the magmatic-hydrothermal processes that formed the deposit. In this study, we investigated the columbite-group minerals and micas in the deposit using SEM, EPMA and LA-ICP-MS trace element mapping techniques to understand the processes responsible for the Ta—Nb mineralization.

2. Geological background

The North China Craton, which lies between the Central Asia Orogenic Belt to the north and the Yangtze Craton to the south (Fig. 1), is composed of an Archean to Paleoproterozoic metamorphic basement overlain by a Mesoproterozoic to Permian platform cover (e.g., Zhai and Santosh, 2011). Its final amalgamation occurred at ca.1.85 Ga (Zhao et al., 2001; Zhao et al., 2005) and later underwent lithospheric thinning and destruction in the early Mesozoic (Xu, 2001; Zhu et al., 2012), leading to large-scale tectonic-thermal events in the early Cretaceous (130–120 Ma) (Wu et al., 2005). The development of the early Cretaceous magmatism, metamorphic core complexes (Davis et al., 2002; Liu

et al., 2005), intracontinental rift basins (Ren et al., 2002) and gold mineralization (Li et al., 2012) in the craton was coeval with the peak stage of its lithospheric thinning and destruction (Zhu et al., 2012).

A number of the early Cretaceous A-type granitic plutons, i.e., Yansaihu, Xiangshan, Jiashan, Qiancengbei, Wulingshan, Madi, Donghouding and Zhaojinggou, were emplaced during extension of the Yinshan-Yanshan fold and thrust belt (Fig. 1), extending up 800 km along the northern margin of the craton (Davis et al., 2002; Yang et al., 2008). The Yansaihu, Xiangshan, Qiancengbei and Wulingshan plutons are arfvedsonite-bearing granites with zircon U—Pb ages of 115 Ma, 116 Ma, 129 Ma and 130 Ma, respectively (Yang et al., 2008; Zeng, 2016). The Jiashan syenite and Donghouding granitic porphyry have ages of 110 Ma and 129 Ma, respectively (Liang et al., 2013; Liu et al., 2015). The Madi and Zhaojinggou albite granites host significant Ta—Nb mineralization (Chai and Wu, 2013; Ye et al., 1991).

The Zhaojinggou Ta—Nb deposit occurs in the westernmost part of the A-type granite belt (Fig. 1). The Ta—Nb mineralization is hosted in a fine-grained, albite granite body, which is about 400 m long and 20 to 100 m wide with a surface exposure of ~0.05 km^2 (Chai and Wu, 2013) (Fig. 2a, b). The granite body and a few wolframite-quartz veins intrude Carboniferous sandstone of the Shuanmazhuang Formation (Fig. 2a), and sandstone breccia commonly occurs along the intrusive contact (Fig. 3a). In cross-section, the granite forms a northeast-
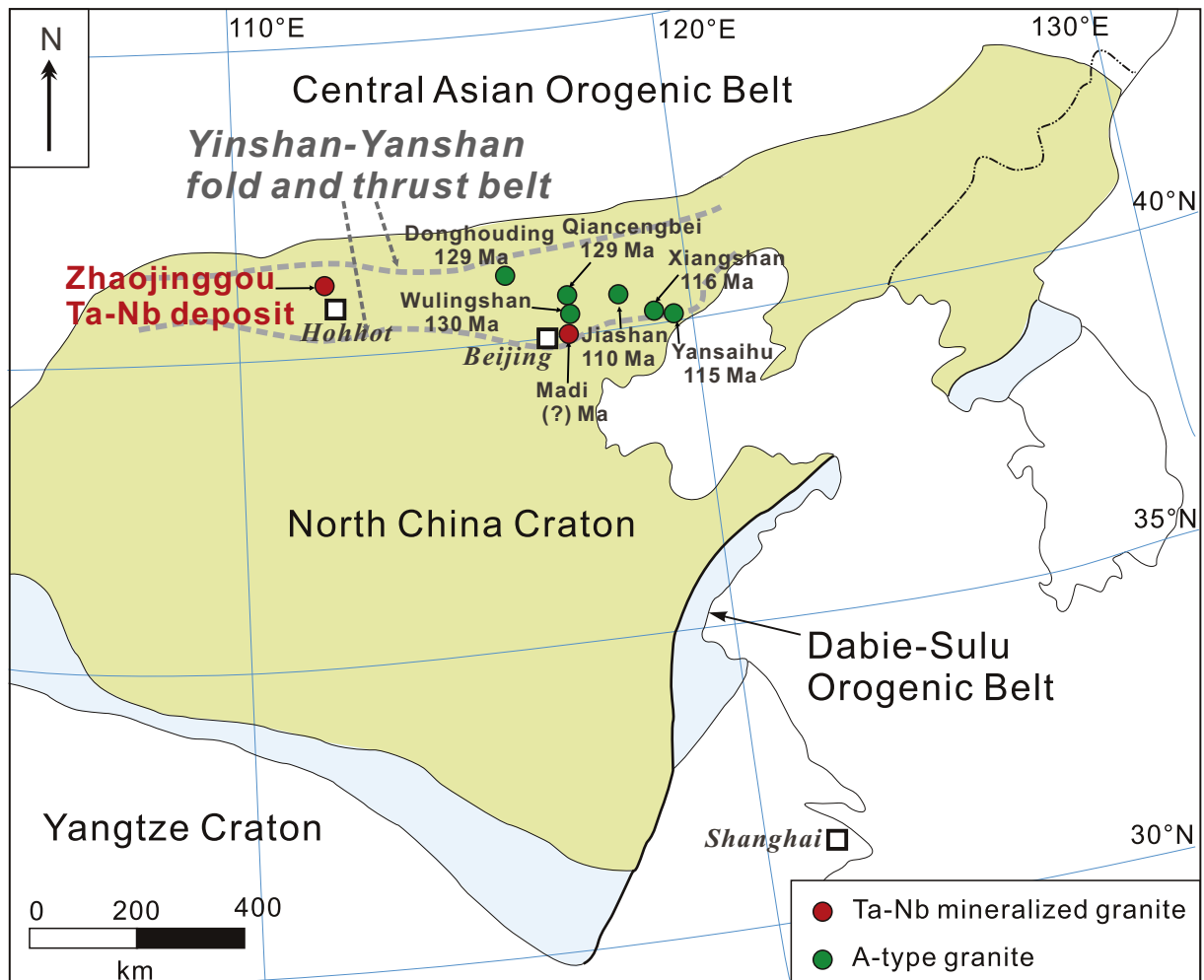

Fig. 1. A simplified geological map showing the distribution of the early Cretaceous Ta—Nb mineralized granites and A-type granites in the northern margin of the North China Craton (modified from Zhu et al., 2012).
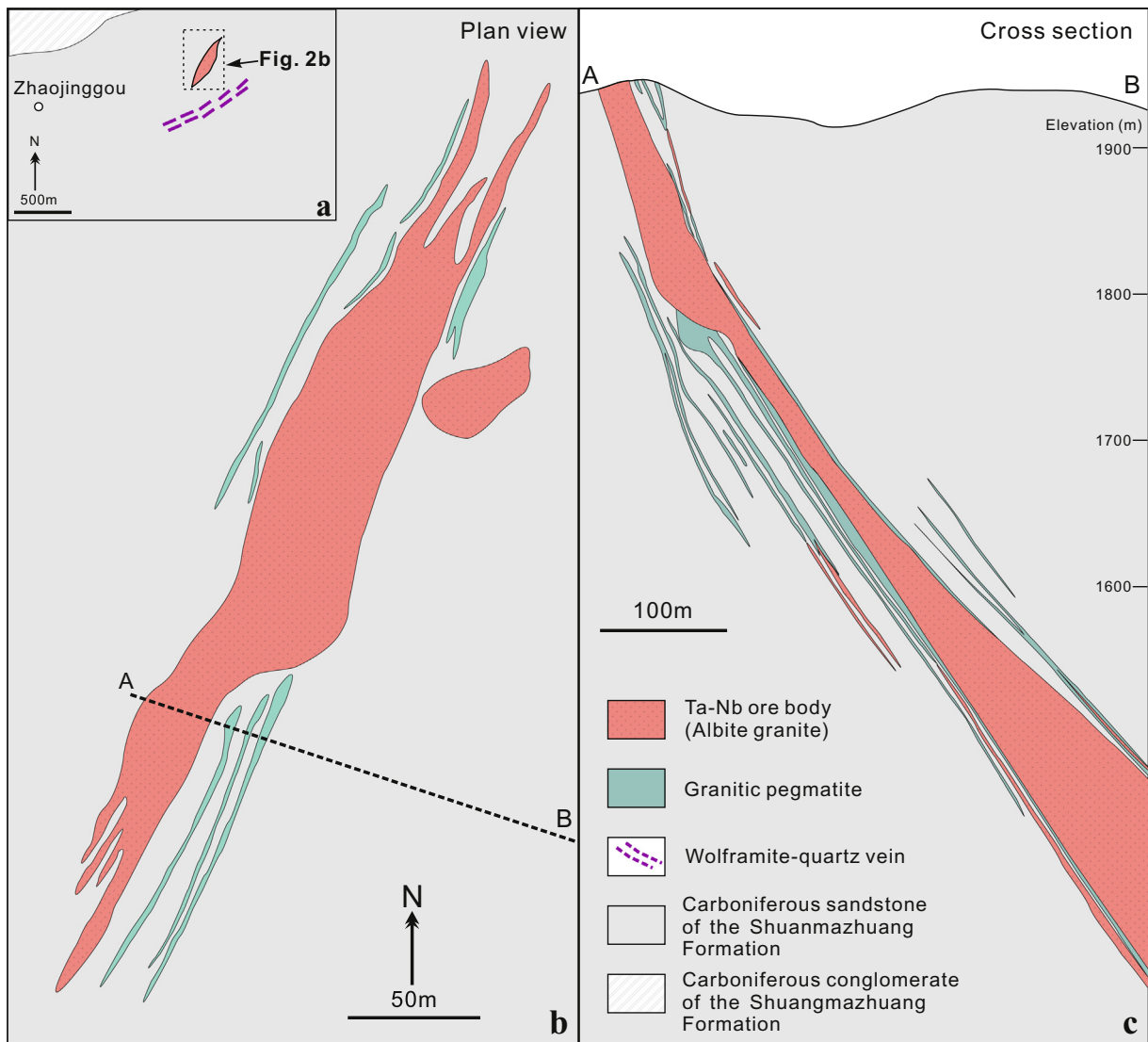
Fig. 2. (a) A simplified geologic map of the Zhaojinggou Ta—Nb deposit. (b) Plan view of the Zhaojinggou Ta—Nb deposit. (c) Cross section of the Zhaojinggou Ta—Nb deposit. (Modified from Chai and Wu, 2013).

striking, dike-like body that dips 50° to 70° SE, and extends to a depth of ~770 m (Fig. 2c). Granitic pegmatites intrude the margin of the granite body along sharp but irregular contacts (Fig. 3c), ranging from several centimeters to meters in width (Fig. 2b, c). Some thin greisen and granitic pegmatite veins also intrude the granite body along its margins (Fig. 3b, d).

3. Analytical methods

3.1. Back-scattered electron (BSE) and cathodoluminescence (CL) imaging

BSE images were obtained from polished thin sections using a Phenom XL scanning electron microscope (SEM) equipped with an energy dispersive spectrometer (EDS) at the Chinese Academy of Science (CAS) Key Laboratory of Mineralogy and Metallogeny, Guangzhou Institute of Geochemistry (GIG). Semi-quantitative EDS was applied to obtain approximate chemical compositions and element maps of minerals.

CL images were obtained from thin sections using a Gatan MonoCL4 system installed on a Carl Zeiss SUPRA 55 SAPPHIRE field emission electron microscope at the State Key Laboratory of Isotope Geochemistry, GIGCAS.

3.2. Mineral composition analyses

Major elements of mica, albite, K-feldspar and columbite-group minerals were determined by electron probe microanalysis (EPMA) using a JEOL JXA-8230 at the CAS Key Laboratory of Mineralogy and Metallogeny. Operating conditions of 15 kV accelerating voltage, 20 nA probe current, and a 3 μm beam were applied to the analyses for all elements. In situ trace element analyses of mica, albite, K-feldspar, and zircon were carried out using an Agilent 7500a inductively coupled plasma-mass spectrometer coupled with a Resonetic 193 nm ArF excimer laser ablation system. Single spot ablation was adopted with a laser beam width of 31 μm. Laser energy was 80 mJ and ablation frequency was 6 Hz. Helium was used as a carrier gas. NIST SRM 610 glass was employed as an external standard, and the SiO_2 contents of mica, albite, and K-feldspar determined by EMPA were used as internal standards.

3.3. Trace element mapping of mica

LA-ICP-MS imaging of trace element distribution within mica was performed at the Ore Deposit and Exploration Center of Hefei University
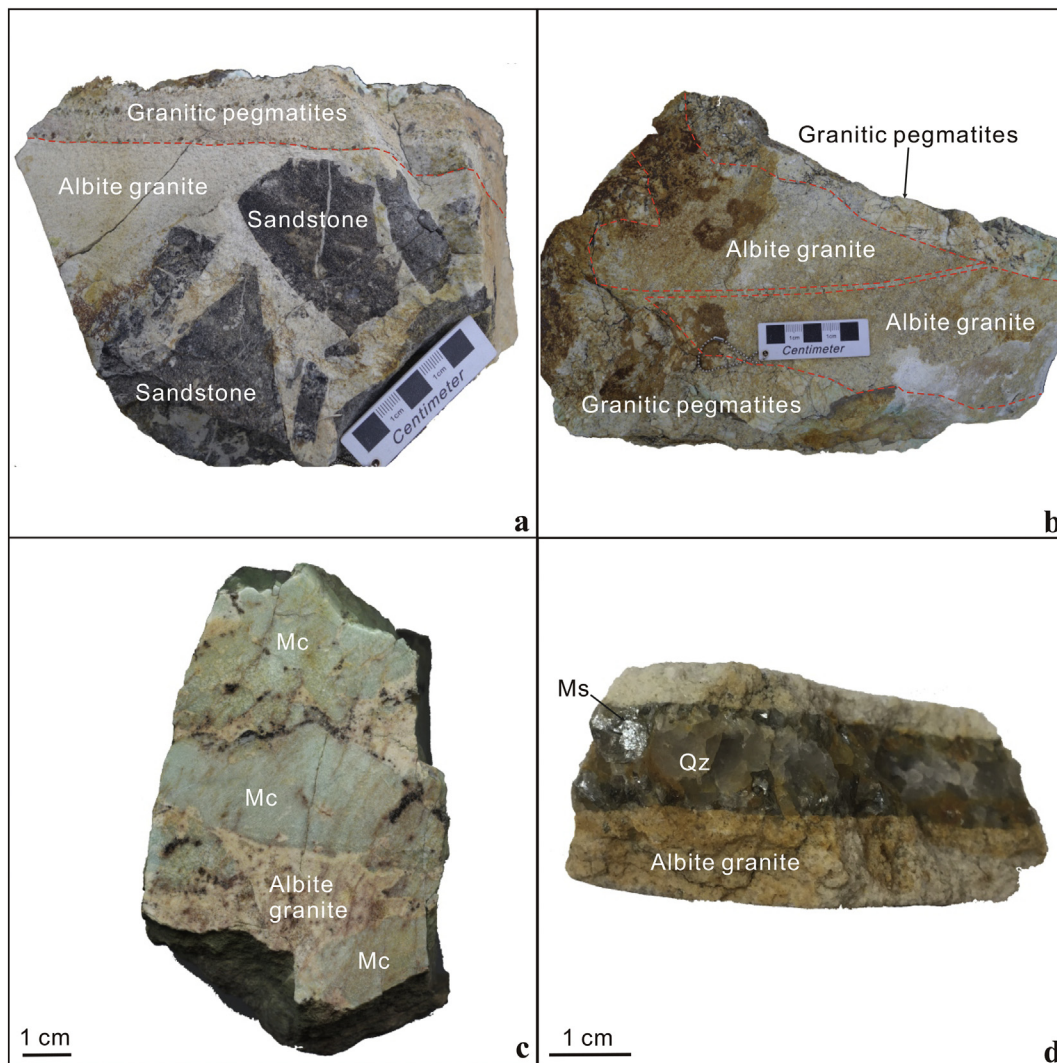
Fig. 3. Hand specimen photographs of the samples from the Zhaojinggou Ta—Nb deposit. (a) Albite granite is fine-grained and contains sandstone breccia, which is cut by granitic pegmatites. (b) Albite granite is cut by granitic pegmatites. (c) Granitic pegmatite with sharp, but irregular contacts with the albite granite. (d) Albite granite is cut by a greisen vein. Abbreviations: Mc = microcline, Ms. = muscovite, Qz = quartz.

of Technology, China, using an Agilent 7900 ICP-MS equipped with a Photon Machines Analyte HE 193 nm ArF excimer laser. Sets of parallel line rasters in a grid across the sample were ablated with a beam of 15 μm and a scanning speed of 15 μm/s. A laser repetition of 10 Hz was selected at a constant energy output of 80 mJ, resulting in an energy density of ~2 J/cm^2 at the target. Reference material GSE-1 g was analyzed at the start and the end of each mapping for data calibration. Images were compiled and processed using LIMS (in-house designed mapping reduction software based on Matlab). For single elements, the average background was subtracted from its corresponding raster, and the rasters were compiled into a 2-D image displaying combined background/drift corrected intensities. A detailed description of the procedure is given in Wang et al. (2017).

3.4. Whole-rock major and trace element analyses

Whole-rock major and trace element analyses were performed at ALS Minerals in Guangzhou, China. The major elements were analyzed by X-ray fluorescence (XRF), with an analytical precision better than ±2–5%. The trace elements were determined by inductively coupled plasma mass spectrometry (ICP-MS) after complete dissolution. The analytical precision for most of the trace elements was better than ±5%.

3.5. U—Pb dating and trace element analyses of columbite-group minerals

The columbite-group minerals were separated using standard heavy liquid and magnetic separation techniques after crushing. The separated grains were then handpicked under a binocular microscope, mounted in epoxy and polished. In situ trace element and U—Pb age analyses were performed at the Institute of Geology and Geophysics, CAS, using a GeoLas PLUS 193 nm excimer ArF laser ablation system coupled to an Agilent 7500a quadrupole-based, inductively coupled plasma mass spectrometer. The minerals were ablated using a spot size of 32 μm and 4 Hz repetition rate. The reference material Coltan 139 was used as an external standard. The fractionation corrections were calculated using GLITTER 4.0 (GEMOC, Macquarie University) and the ages were calculated by IsoplotR (Vermeesch, 2018). Trace element compositions of the minerals were calculated by GLITTER 4.0, with ^{55}Mn as an internal standard and NIST 610 as an external reference material. Detailed descriptions of the procedure are given in Che et al. (2015).

4. Petrography

The albite granite is fine-grained and consists of 65–70 vol% albite, 10–15 vol% K-feldspar, 10–15 vol% quartz, 5–10 vol% mica,

and minor fluorite (1–3 vol%). The grain size ranges from 0.2 to 0.5 mm (Fig. 4a), and the K-feldspar, quartz, mica and fluorite are all interstitial to the larger albite laths. Mica shows irregularly patchy zoning in the BSE images and contains areas of intergrown zinnwaldite and muscovite (Fig. 4a, b).
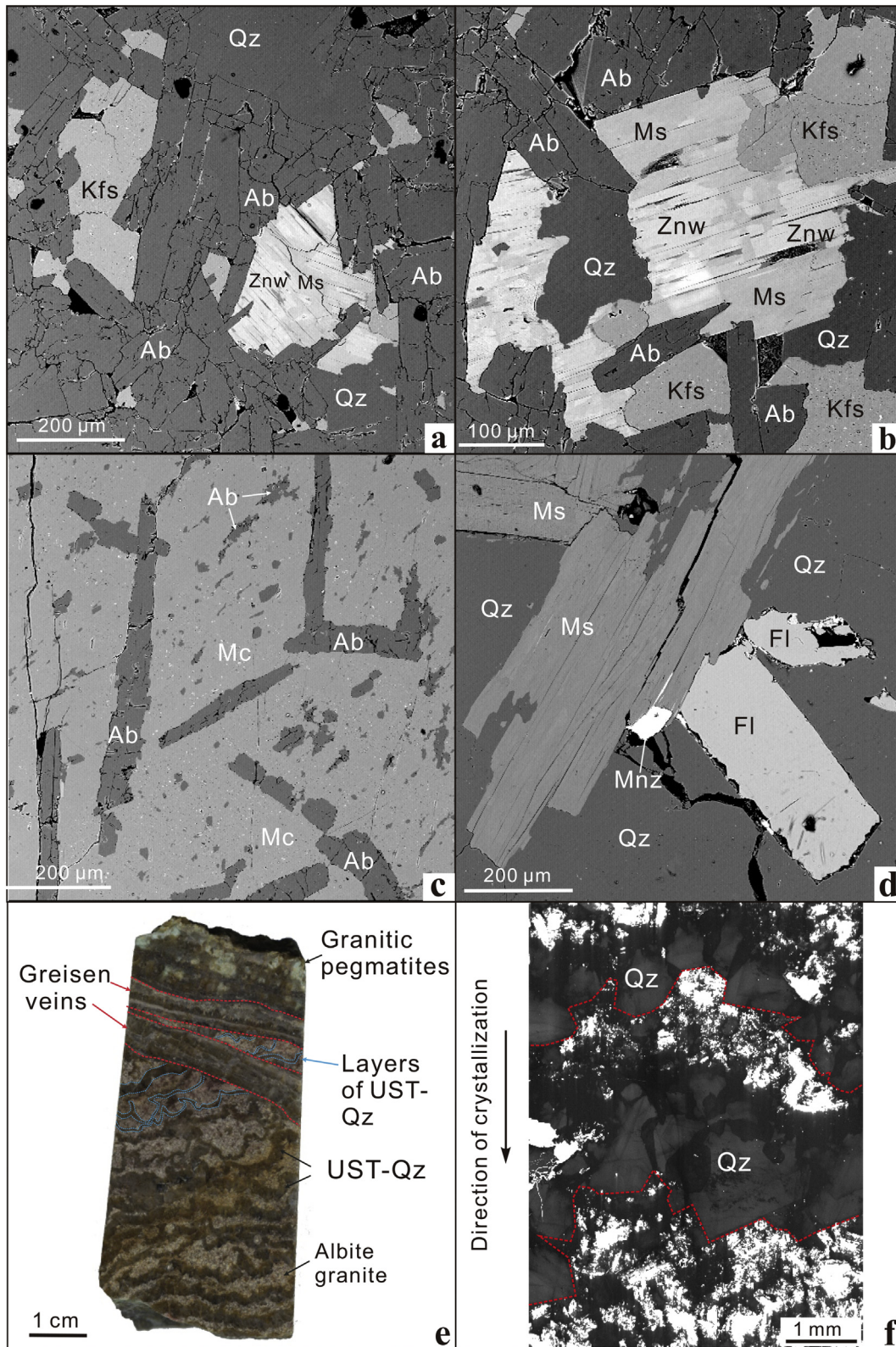

Fig. 4. Petrography of the rocks of the Zhaojinggou Ta—Nb deposit. (a) K-feldspar (Kfs), zinnwaldite (Znw), muscovite (Ms) and quartz (Qz) are interstitial to albite (Ab) in a BSE image of albite granite. (b) BSE image of irregular zoning of mica in the granite. (c) Two types of albite enclosed within microcline (Mc) in a BSE image of granitic pegmatite. (d) The BSE image of a greisen vein consisting of quartz, muscovite, and euhedral fluorite (Fl). (e) The rhythmic layers of quartz with unidirectional solidification textures (UST) which are cut by greisen veins and granitic pegmatites. (f) The CL image of quartz in the UST texture grows in one direction. The black arrow shows the direction of crystallization.

Granitic pegmatite consists of blue or pale-green microcline, albite and minor quartz. Albite is enclosed within the microcline and appears as either irregular patches or oriented laths (Fig. 4c). Associated greisen consists of muscovite, quartz and minor fluorite (Fig. 4d). Small grains of monazite in the greisen veins locally fill angular interstices among muscovite, fluorite and quartz (Fig. 4d).

Distinctive quartz-rich, unidirectional solidification textures (UST) occur in the margin of granite body. Rhythmic and crenulate layers of quartz alternate with fine-grained albite granite, showing a so-called "brain rock" texture (Shannon et al., 1982) (Fig. 4e). Each quartz layer ranges in thickness from 1 to 3 mm and is cut by the greisen veins and granitic pegmatites (Fig. 4e). Crystals in the crenulate layers consist of quartz and minor zinnwaldite, both of which are much coarser than the grains in the adjacent granite. The quartz grains in the crenulate layers display an irregular shape on one side and euhedral, hexagonal crystal terminations on the
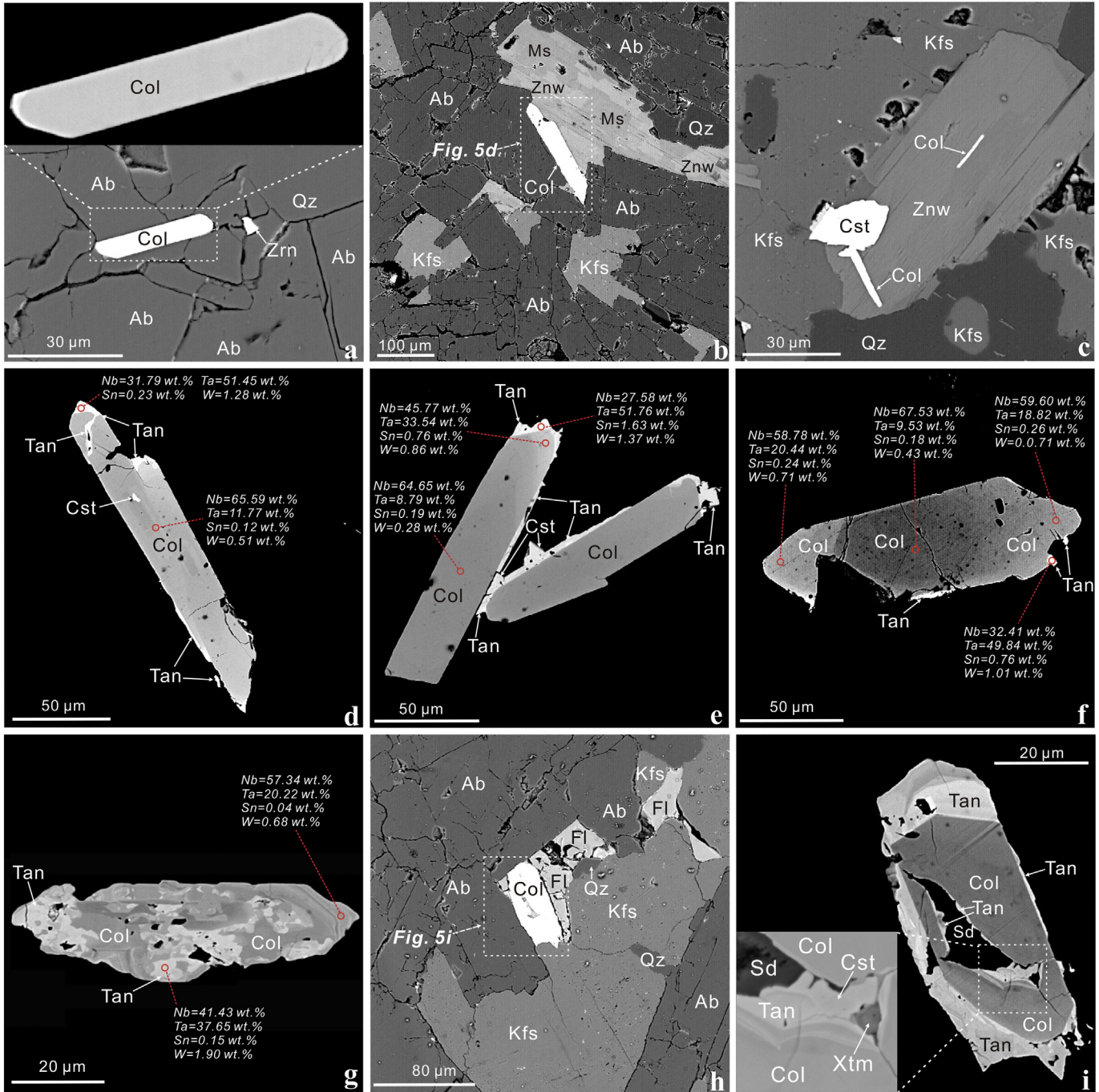

Fig. 5. BSE images of columbite-group minerals. (a) Fine-grained and platy columbite (Col) and zircon (Zrn) are interstitial to albite (Ab) and quartz (Qz). The columbite in inset displays no zoning. (b) Zinnwaldite (Znw) and muscovite (Ms) are interstitial to coarse-grained, euhedral columbite, albite and quartz. (c) Columbite and cassiterite (Cst) enclosed within the zinnwaldite. (d) Close-up of the columbite-group minerals in Fig. 5b showing that irregular tantalite (Tan) penetrates the euhedral columbite. (e) Columbite grains are rimmed by irregular tantalite and subhedral cassiterite. (f) Euhedral, prismatic columbite has small patches of tantalite in the margin. (g) Irregular tantalite patches in columbite. Note that the columbite preserves oscillatory zoning on its right edge. (h) Euhedral, prismatic columbite and fluorite (Fl) are interstitial to albite and K-feldspar (Kfs). (i) Close-up of the columbite in Fig. 5h showing penetration of euhedral prismatic columbite grains by irregular tantalite, cassiterite, siderite (Sd) and xenotime (Xtm) along the fractures and edges; The inset is a close-up of prismatic columbite.

other side, showing a downward direction of crystallization (Fig. 4f).

5. Texture of columbite-group and rare element-bearing minerals

5.1. Columbite-group minerals

Columbite-group minerals in the Zhaojinggou deposit, which are hosted in the albite granite, are mainly Ta-Nb-rich phases that occur as disseminated, euhedral grains (Fig. 5). Fine-grained columbite-

group minerals (<100 μm) are typically platy with weak to no zoning in their BSE images (Fig. 5a and close-up inset), whereas coarse-grained varieties (>100 μm) are typically prismatic (Fig. 5b). They are commonly interstitial to albite, or rarely, enclosed within zinnwaldite (Fig. 5c).

Coarse-grained columbite-group minerals display diverse zoning patterns (Fig. 5d–i); some grains are entirely columbite showing oscillatory zoning that are partly rimmed by irregular tantalite and cassiterite, whereas others have patchy textures (Fig. 5d–f). Columbite domains are locally penetrated by tantalite grains (Fig. 5d) and some columbite
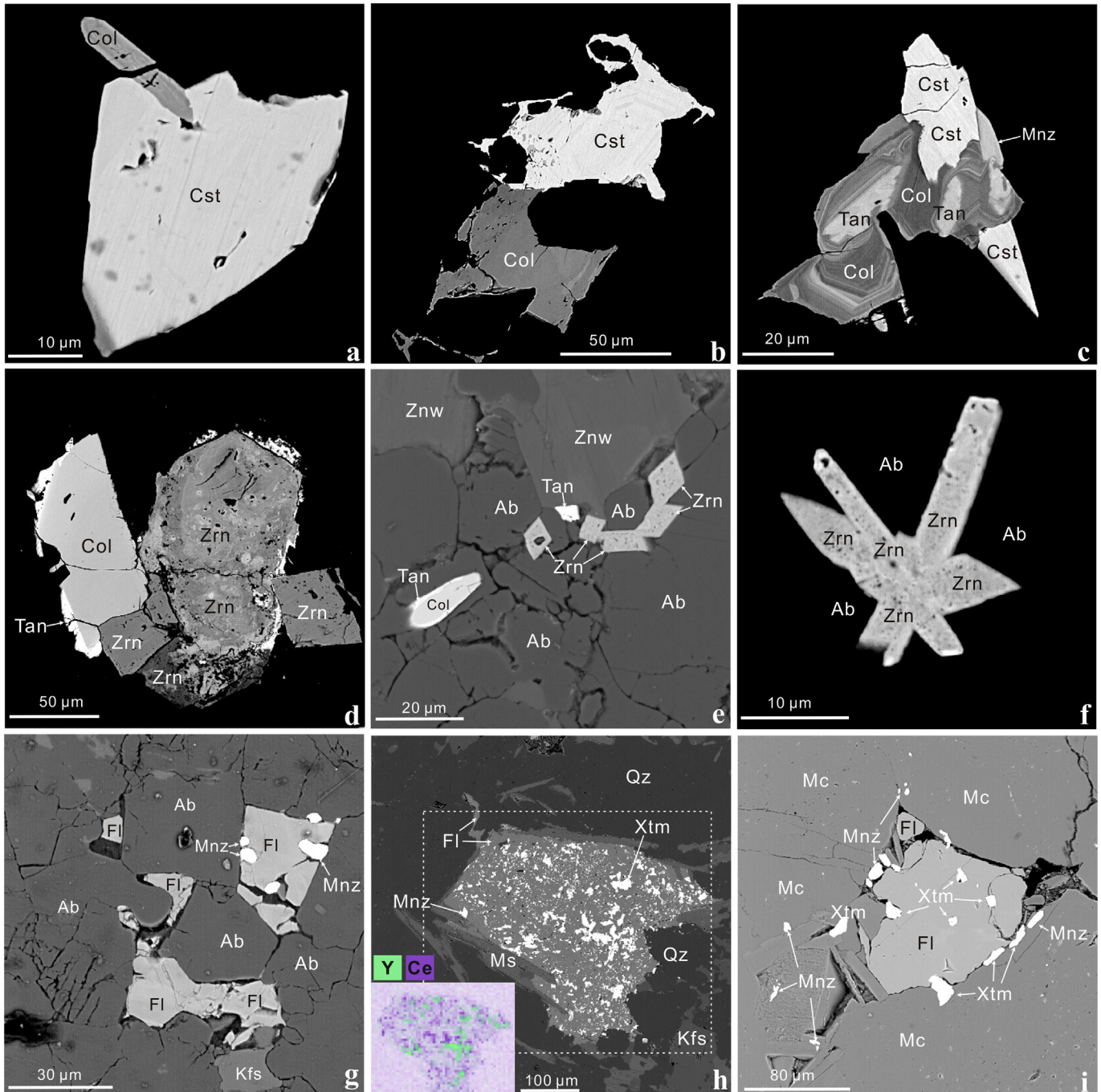

Fig. 6. BSE images of cassiterite, REE-bearing minerals, and zircon. (a) Intergrowth of subhedral cassiterite (Cst) and euhedral columbite (Col). (b) Intergrowth of anhedral cassiterite and columbite in albite granite. (c) Intergrowth of subhedral cassiterite, monazite (Mnz), tantalite (Tan), and columbite in the granite. (d) Aggregates of euhedral metamict zircon (Zrn) in the granite. (e) Zircon aggregates associated with tantalite and columbite in the granite. (f) Flower-like zircon aggregates in the granite. (g) Monazite enclosed within fluorite (Fl) that is interstitial to albite in the granite. (h) Disseminated monazite and xenotime (Xtm) enclosed within fluorite in a greisen vein. Colorized EDS elemental mapping shows the distribution of Y and P in selected areas (dotted box). (i) Monazite and xenotime are associated with the fluorite that is interstitial to microcline in granitic pegmatite.

grains are replaced by patchy tantalite (Fig. 5g). Grains enclosed in fluorite (Fig. 5h) show a homogeneous columbite core, which is surrounded by banded tantalite (Fig. 5i) or penetrated by tantalite, cassiterite, and xenotime along micro-cracks (Fig. 5i and close-up inset).

5.2. Rare element-bearing minerals

Cassiterite and zircon are commonly intergrown with columbite-group minerals in the albite granite (Fig. 6a–f), and aggregates of cassiterite, columbite, and monazite may also occur as interstitial phases (Fig. 6b,c). Zircon aggregates are locally present in the granite and some grains in the aggregates show distinct dissolution textures with pores and cracks (Fig. 6d). Some euhedral zircon aggregates are enclosed within albite (Fig. 6e,f).

Monazite and xenotime are common REE-bearing phases in the granite, typically associated with fluorite (Fig. 6g–i). Most grains are interstitial to albite in the granite (Fig. 6g), to quartz in the greisen veins (Fig. 6h), and to microcline in the granitic pegmatites (Fig. 6i).

6. Mineral compositions

6.1. Mica

Mica in the albite granite displays complex zoning patterns with interlocking dark and bright domains in the BSE images (Fig. 4a, b); the dark domains contain ~2 to 3 wt% F and are mainly muscovite, whereas the bright domain contain ~7 wt% F and are mainly zinnwaldite (Supplementary Table 1). Mica in the UST layers is zinnwaldite, whereas that in the greisen veins is muscovite (Fig. 7). Zinnwaldite in the UST layers contains 352–512 ppm Nb, 79–142 ppm Ta, and 1428–2877 ppm Sn, much higher values than those of zinnwaldite in the granite (Fig. 8a,b,d). Muscovite in the granite and greisen veins has much higher W and Ba than those of zinnwaldite in the granite and UST layers (Fig. 8e,g).

A mica grain with distinct zoning in the albite granite (Fig. 9a) was selected for LA-ICP-MS trace element mapping. The results show that Fe, Li, Rb, Nb, Ta, and Pb are enriched in the zinnwaldite domain (Fig. 9b–g), and that Al, Mn, Ba, Sn and W are enriched in the muscovite domain (Fig. 9h–l).

6.2. Microcline and albite

Microcline in the granitic pegmatite is similar in composition to the K-feldspar in the granite. These feldspars contain 65 wt% SiO_2, 17 to 18 wt% Al_2O_3, 16 to 17 wt% K_2O, and < 0.6 wt% Na_2O (Supplementary Table 2). Both are rich in Rb (2800 to 5500 ppm). Irregular albite grains and albite laths in the granitic pegmatite also have major and trace element compositions very similar to albite in the granite (Supplementary Table 3). In addition, microcline and albite in the granitic pegmatite have REE concentrations below the detection limit of the LA-ICP-MS.

6.3. Columbite-group minerals

Columbite grains in the albite granite display some enrichment in Ta—Mn on the plot of Ta/(Ta + Nb) versus Mn/(Mn + Fe) (Fig. 10a), and the tantalite that rims the columbite grains has much higher Ta concentrations than the columbite. The euhedral columbite grains show the enrichment of HREE on the chondrite-normalized REE patterns (Fig. 10b), but have highly and variable LREE concentrations (Supplementary Table 4).

6.4. Zircon

Zircon grains in the albite granite are metamict (Fig. 11a) and cannot be used to constrain meaningful U—Pb ages. They have elevated LREE concentrations relative to those of magmatic zircon (Supplementary Table 5), and have chondrite-normalized REE patterns similar to those of hydrothermal zircon (Fig. 11a). On the diagrams of Ce anomaly (Ce/Ce*) versus $(Sm/La)_N$ and $(Sm/La)_N$ versus La, they plot close to the field of hydrothermal zircon (Fig. 11b and c).

7. Whole-rock compositions

The samples of albite granite contain 73.5 to 77.0 wt% SiO_2, 12.5 to 18.4 wt% Al_2O_3, 7.8 to 9.8 wt% ($Na_2O + K_2O$) and have less than 0.2 wt% CaO (Table 1). They are peraluminous with ACNK [Al_2O_3/(CaO + Na_2O + K_2O)] values of 1.07 to 1.13 and ANK [Al_2O_3/(Na_2O + K_2O)] values of 1.08 to 1.14 (Fig. 12).

All the samples from the Zhaojinggou Ta—Nb deposit show fractionated LREE/HREE, chondrite-normalized REE patterns with negative Eu anomalies (Eu/Eu* = 0.07–0.28), and distinct M-type
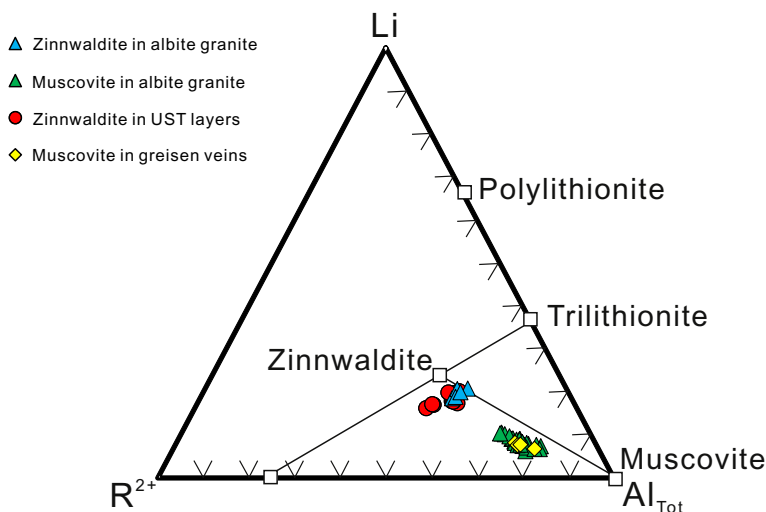

Fig. 7. Classification of mica in the Zhaojinggou Ta—Nb deposit (after Foster, 1960). Li and H_2O in the mica was calculated based on the method of Monier and Robert, 1986 and Tindle and Webb, 1990, respectively.

lanthanide tetrad patterns (Fig. 13a) with TE$_{1,3}$ (evaluation of the tetrad effect, after Irber, 1999) ranging from 1.2 to 1.5 (Fig. 14a). They are also very depleted in Ba, Sr, Eu and Zr, and enriched in Cs, Rb, W, Nb, Ta, Pb, Sn and Li (Fig. 13b). The granitic pegmatites have much lower Nb, Ta, Zr, and Sn concentrations than other rock types. All the rocks have Nb/Ta values less than 4 (Fig. 14a) and Zr/Hf values less than 10 (Fig. 14b).

8. Columbite U—Pb ages

Columbite grains from three albite granite samples were analyzed for U—Pb ages (Supplementary Table 6). 18 spots for sample ZJ-1 gave a lower intercept age of 134.6 ± 2.1 Ma (2σ, n = 18, MSWD = 1.5) on the Tera-Wasserburg concordia diagram (Fig. 15a), 36 spots for sample ZJ-6 yielded a lower intercept age of 133.3 ± 0.9 Ma (2σ,
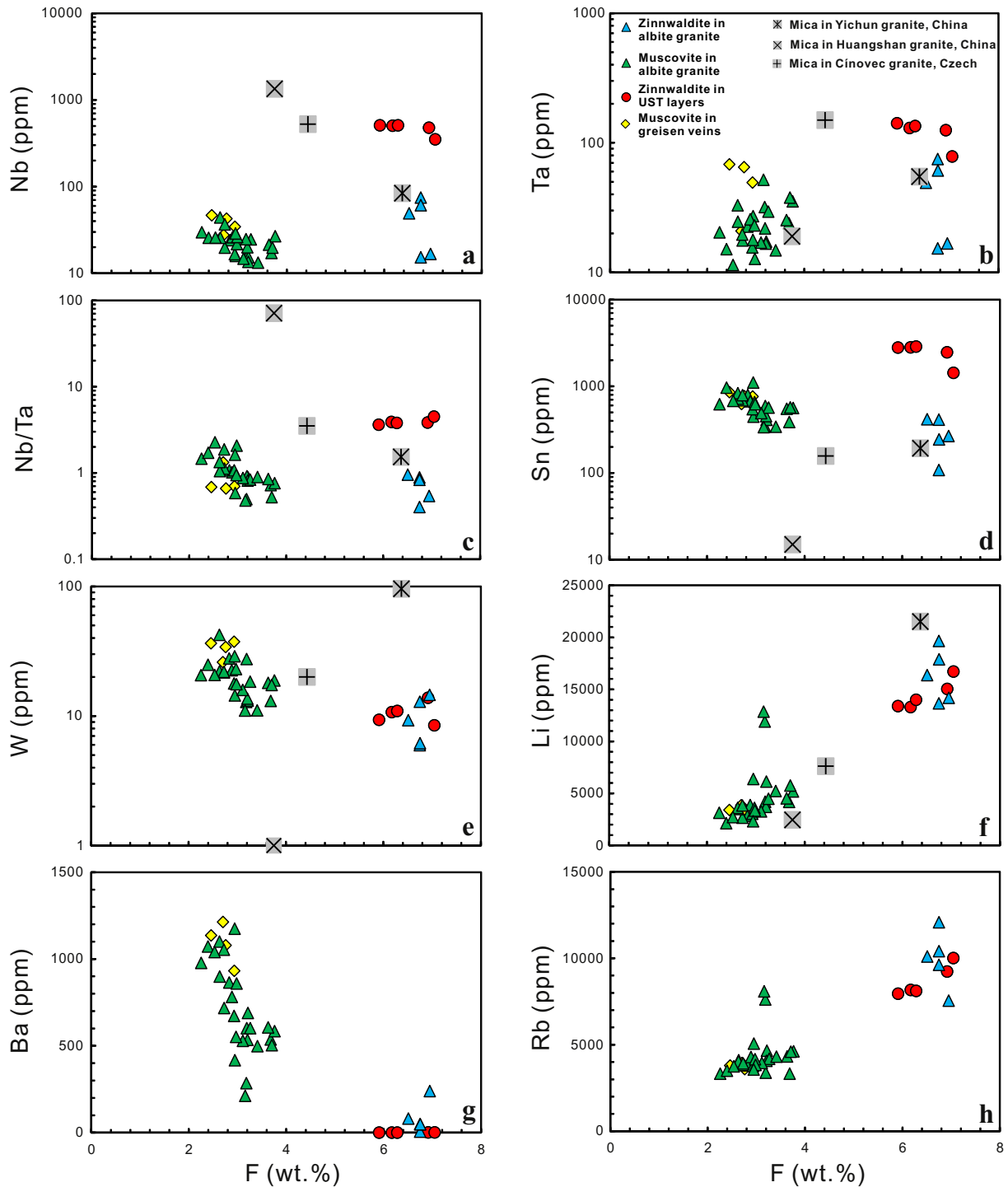

Fig. 8. Plots of (a) Nb, (b) Ta, (c) Nb/Ta, (d) Sn, (e) W, (f) Li, (g) Ba, and (h) Rb vs. F of mica in the Zhaojinggou Ta—Nb deposit compared with other ore bodies. Data sources: the Yichun granite (Li et al., 2015), the Cínovec granite (Johan et al., 2012), and Huangshan granite (Zhu et al., 2018).

$n = 36$, MSWD = 1.5) (Fig. 15b) and 25 spots for sample ZJ-8 yielded a lower intercept age of 131.8 ± 1.0 Ma (2σ, $n = 25$, MSWD = 1.8) (Fig. 15c). The three obtained ages are consistent with each other, and can be considered to be the crystallization age of columbite.

9. Discussion

9.1. Timing of Ta—Nb mineralization in the Zhaojinggou deposit

The mineralization age of the Zhaojinggou Ta—Nb deposit has been debated since it was discovered in 2012. The first zircon U—Pb age for the deposit was reported to be 277 ± 2 Ma (Nie et al., 2013), although this was only mentioned in the abstract with no data. Later, an ^{40}Ar—^{39}Ar age of muscovite from the granitic pegmatite was reported to be 124.0 ± 2.0 Ma (Gao et al., 2017), which is nearly coeval with a zircon U—Pb age of 125 ± 1 Ma and four monazite U—Pb ages ranging from 121 ± 1 Ma to 124 ± 2 Ma for the albite granite (Li et al., 2019). Most recently a biotite ^{40}Ar—^{39}Ar age of 133 ± 1 Ma for a biotite-quartz vein was reported by Li et al. (2019).

Because the columbite-group minerals are the main Ta-Nb-rich phases in the deposit, we suggest that their U—Pb ages provide the best estimate for the timing of mineralization. Columbite U—Pb ages
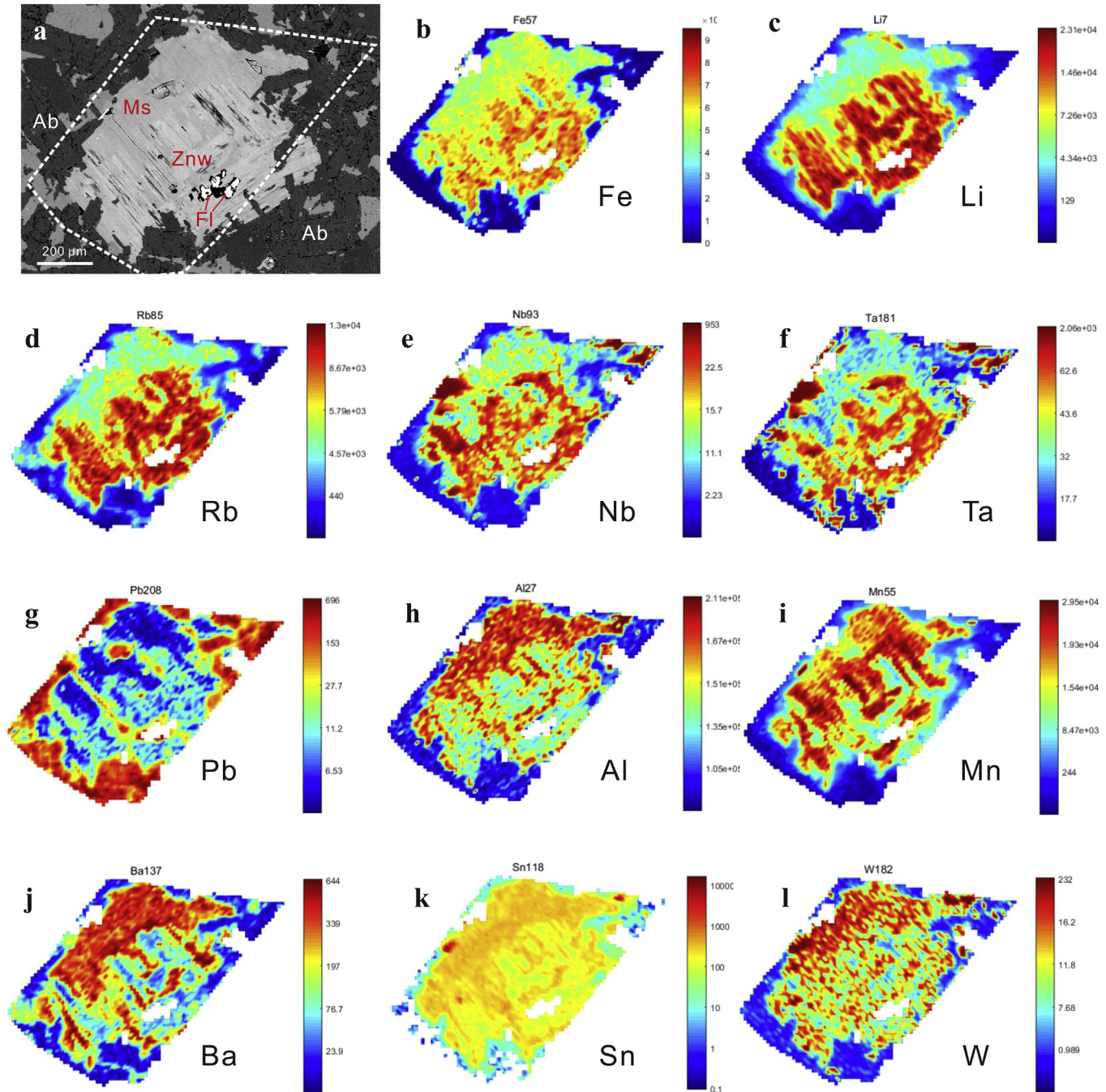

Fig. 9. BSE images and LA-ICP-MS trace element mapping for mica in the albite granite. (a) Mica shows irregular zoning patterns with bright domains of F-rich zinnwaldite (Znw) and dark domains of F-poor muscovite (Ms). (b–l) Trace element mapping showing that Fe, Li, Rb, Nb, Ta and Pb are enriched in the bright domains (b to g), and Al, Mn, Ba, Sn and W are enriched in the dark domains (h to l). The dotted lines show the analyzed areas.

obtained in this study range from 131.8 ± 1.0 Ma to 134.6 ± 2.1 Ma, close to the ages reported by Li et al. (2019) and Gao et al. (2017), indicating that the Ta—Nb mineralization occurred in the early Cretaceous.

Voluminous magmatism, extensional deformation and associated gold mineralization in the early Cretaceous was coeval with the peak of lithospheric thinning and destruction of the North China Craton (e.g., Wu et al., 2005; Xu, 2001; Zhu et al., 2012). The Ta—Nb mineralization of the Zhaojinggou deposit was also coincident with this significant tectonic-thermal event. The Ta—Nb mineralization was likely related to emplacement of the coeval A-type granitic plutons along the Yinshan-Yanshan fold and thrust belt (Fig. 1). They all occurred in an extensional setting due to the large-scale lithospheric thinning (e.g., Yang et al., 2008).

In addition to the Zhaojinggou Ta—Nb deposit, the Madi granitic pluton in the eastern part of the Yinshan-Yanshan also contains significant Ta—Nb mineralization (Ye et al., 1991) (Fig. 1). Although the age of

Ta—Nb mineralization in the Madi granitic pluton has not yet been confirmed, it likely formed in a similar extensional setting because the Madi pluton is adjacent to the Qiancengbei and Wulingshan A-type granitic plutons, both of which have the crystallization ages of ca. 130 Ma (Yang et al., 2008; Zeng, 2016) (Fig. 1).

9.2. Peraluminous granite host of the Zhaojinggou Ta—Nb deposit

In the Zhaojinggou deposit, the albite granite body is about 20 to 100 m wide, whereas the granitic pegmatites are several centimeters to meters wide (Fig. 2). The pegmatites are located along the boundary between the granite pluton and its wall rocks and have irregular, but sharp contacts with the granite (Fig. 3). This suggests that the granite pluton may be a large, buried body from which the pegmatites were derived. The granite hosting the Ta—Nb ore bodies contains 80 to 110 ppm Nb and 40 to 170 ppm Ta, whereas the pegmatites are nearly barren in
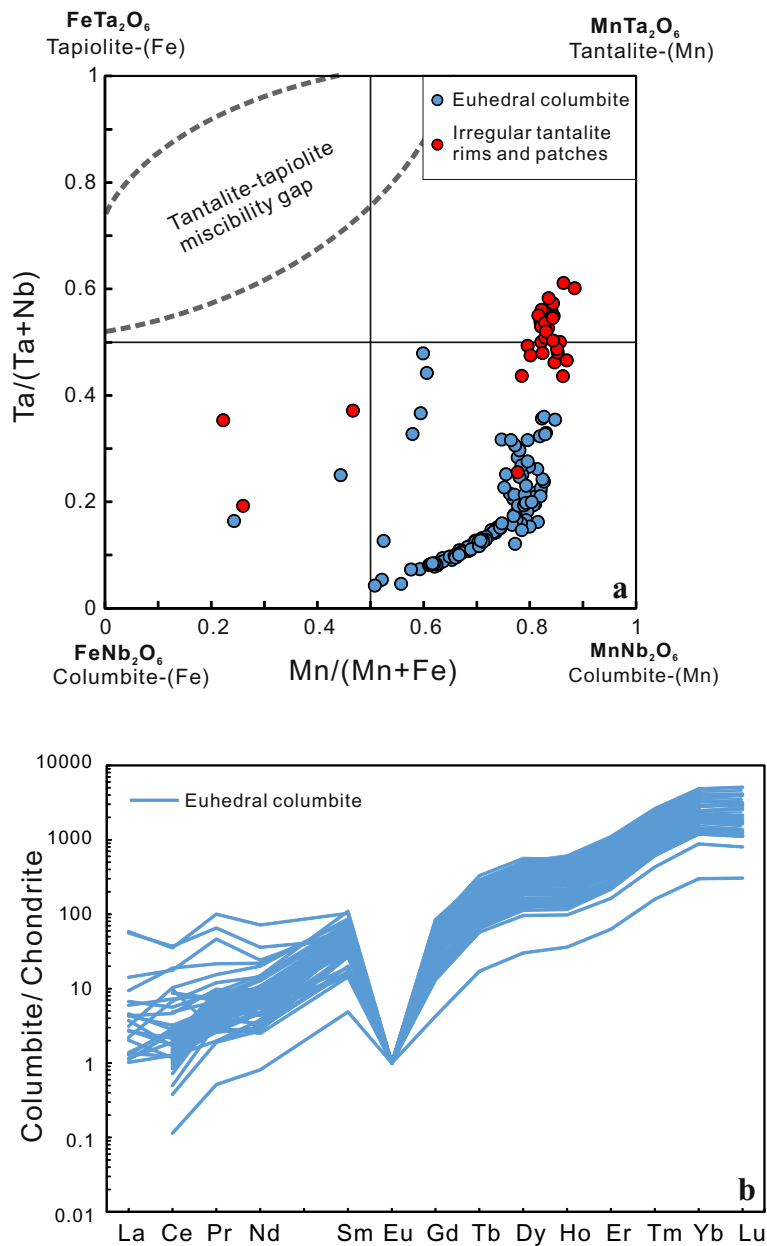

Fig. 10. (a) Plot of Ta/(Nb + Ta) vs Mn/(Mn + Fe) of columbite-group minerals (modified from Černý et al., 1992); (b) Chondrite-normalized REE patterns of columbite-group minerals. The normalization values are from Sun and McDonough (1989).

these elements with only 0.6 to 7.7 ppm Nb and 0.6 to 4.9 ppm Ta (Fig. 13b and Table 1). Although the granite is fine-grained, it is unlikely to be a border zone of the pegmatites (c.f., London, 2014).

The granite is peraluminous with high SiO$_2$ (73.5 to 77.0 wt%) and total alkalis (Na$_2$O + K$_2$O = 7.8–9.8 wt%) (Fig. 12 and Table 1), indicating high degrees of fractional crystallization of the parental magma

(Pollard, 1986). All the granite samples in this study have Nb/Ta values less than 4 (Fig. 14a) and Zr/Hf less than 10 (Fig. 14b), consistent with other typical Ta-Nb-mineralized peraluminous granites (Ballouard et al., 2016). The presence of disseminated columbite-group minerals and high-Li mica in the granite (Fig. 5a, 8f) is also consistent with the features of other Ta—Nb deposits hosted in peraluminous granites
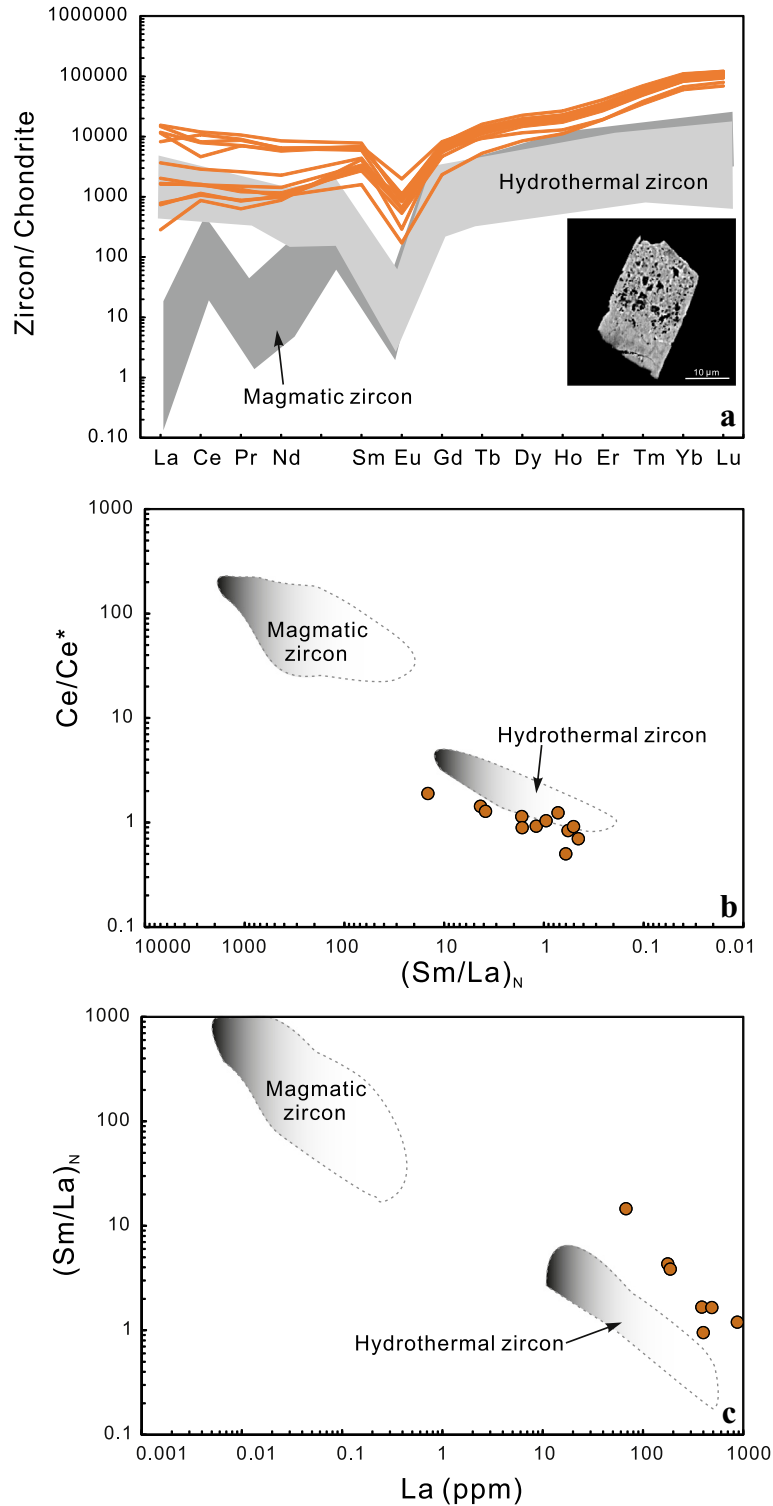
Fig. 11. (a) Chondrite-normalized REE patterns of zircon in the albite granite. The inset BSE image shows an intense dissolution texture of the metamict zircon with pores and cracks. The reference areas of magmatic and hydrothermal zircon are after Yang et al. (2014). (b) Plot of Ce anomaly (Ce*) vs (Sm/La)$_N$ and (c) plot (Sm/La)$_N$ vs La of zircon. Reference areas for hydrothermal and magmatic zircon are adopted from Hoskin (2005).

Table 1
Major oxides and trace elements contens of the rocks from Zhaojinggou Ta—Nb deposit.

| Sample No.	ZJ-10	ZJ-7	ZJ-2	ZJ-6-1	ZJ-13	ZJ-12	ZJ-6	ZJ-9
Rock types	Albite granite	Albite granite	Albite granite	Albite granite	Granitic pegmatite	Granitic pegmatite	Greisen veins	UST layers
SiO_2 (wt%)	77.0	76.8	73.5	73.5	64.9	66.4	85.7	81.5
TiO_2	<0.01	<0.01	<0.01	<0.01	<0.01	<0.01	0.0	<0.01
Al_2O_3	12.7	12.5	15.3	15.9	18.4	17.3	5.4	8.7
$Fe_2O_3^T$	1.6	1.4	0.6	0.9	0.5	0.6	4.2	2.5
MnO	0.1	0.1	0.1	0.1	0.0	0.0	0.2	0.1
MgO	0.0	0.0	0.0	0.0	0.0	0.0	0.1	0.0
CaO	0.1	0.1	0.1	0.1	0.0	<0.01	0.1	0.1
Na_2O	4.8	4.8	6.3	7.8	2.1	1.7	0.1	1.0
K_2O	3.5	3.0	3.5	1.0	12.9	12.6	2.0	4.3
P_2O_5	0.01	0.02	<0.01	0.01	<0.01	<0.01	<0.01	<0.01
F	0.2	0.1	0.1	0.2	<0.1	0.1	0.6	0.7
LOI	0.2	0.5	0.4	0.6	0.3	0.4	0.9	0.8
Total	100.2	99.3	99.8	100.1	99.1	99.0	99.3	99.6
Li (ppm)	237	165	91	63	10	18	540	940
Be	6.2	4.8	5.4	5.9	6.7	6.5	8.4	5.2
Sc	0.4	0.2	0.1	0.3	0.1	0.1	0.9	0.4
Rb	653	658	919	213	3820	3580	701	1360
Sr	24.2	43.2	14.8	25.9	5.0	9.4	10.1	19.5
Y	31.0	10.1	3.2	9.2	1.8	2.0	15.7	9.9
Zr	85.0	20.0	14.0	38.0	2.0	2.0	24.0	13.0
Nb	97.1	81.2	79.8	112.5	0.6	7.7	25.7	43.7
Sn	6.0	285.0	30.0	34.0	1.0	3.0	83.0	204.0
Cs	4.5	4.3	3.1	3.1	11.0	9.6	10.8	11.0
Ba	25	77	30	35	22	45	205	80
La	15.1	3.3	1.4	2.8	1.0	0.9	1.6	3.0
Ce	47.2	16.0	7.8	10.8	6.0	5.4	9.6	18.2
Pr	6.8	2.9	1.0	2.0	0.6	0.8	1.3	3.3
Nd	22.4	8.9	2.7	5.6	1.7	2.3	3.9	9.0
Sm	5.8	3.3	0.8	1.8	0.5	0.7	1.7	3.4
Eu	0.13	0.06	0.04	0.06	0.04	0.05	0.04	0.06
Gd	3.8	1.6	0.3	1.2	0.3	0.3	1.4	1.8
Tb	0.7	0.5	0.1	0.3	0.1	0.1	0.4	0.6
Dy	4.6	3.5	0.8	2.2	0.5	0.6	3.5	4.1
Ho	0.9	0.7	0.2	0.4	0.1	0.1	0.8	0.7
Er	3.3	2.2	0.7	1.7	0.3	0.4	2.8	2.6
Tm	0.7	0.6	0.2	0.5	0.1	0.1	0.7	0.6
Yb	6.6	5.1	1.8	4.3	0.6	0.7	6.2	5.2
Lu	1.0	0.8	0.3	0.7	0.1	0.1	0.9	0.7
Hf	11.9	4.7	3.6	9.0	0.3	0.5	6.3	3.4
Ta	42.7	47.4	169.5	58.1	0.6	4.9	22.5	23.5
W	6.0	28.0	5.0	7.0	2.0	5.0	98.0	29.0
Pb	77	125	145	136	505	427	182	89
Th	25.3	25.1	3.6	39.9	0.3	0.8	15.2	7.7
U	1.8	1.2	1.6	1.2	<0.05	0.1	1.2	0.7
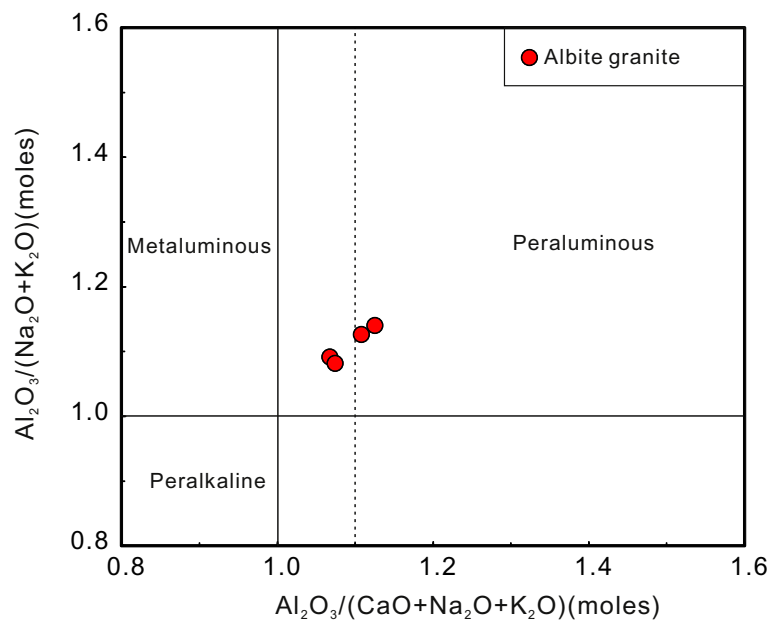
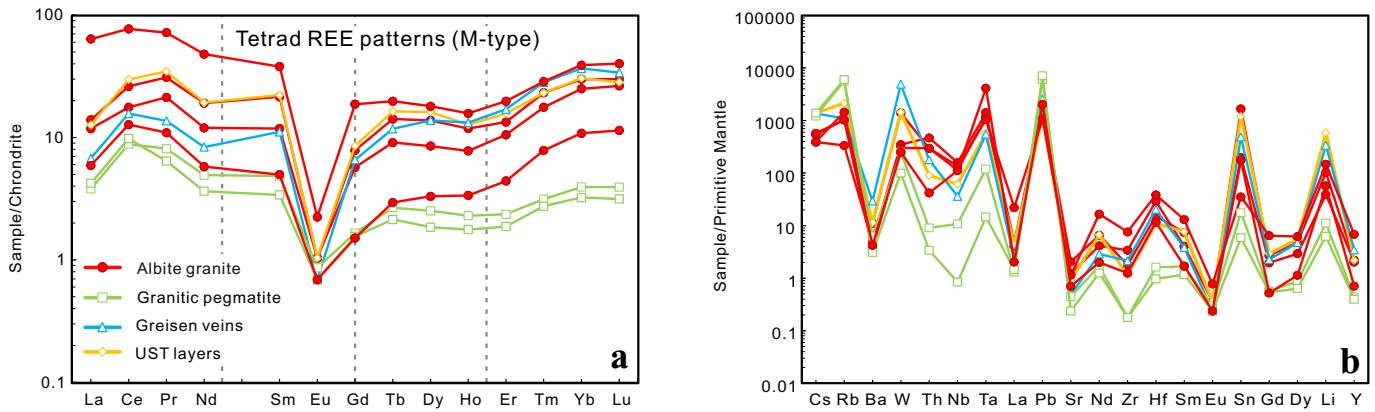**Fig. 12.** Plot of A/NK vs. A/CNK of the albite granite.

Fig. 13. Chondrite-normalized rare earth element patterns (a) and primitive mantle-normalized trace element patterns (b) of the rocks from the Zhaojinggou Ta—Nb deposit. Normalization values are from Sun and McDonough (1989).

(Linnen et al., 2014; Linnen and Cuney, 2005). The Zhaojinggou granite body has a surface exposure of only 0.05 km² and consists of a sole lithology, which is very different from the Yichun granite that has an outcrop area of about 9.5 km² and multiple intrusive units (Huang et al., 2002; Li et al., 2015). Thus, we suggest that the fine-grained granite may represent a highly evolved, apical unit of a larger granitic pluton.

9.3. Magmatic-hydrothermal processes recorded in mica

The UST textures in granites are typically thought to have been generated by undercooling of silicic magma (London, 2009). Mica in the UST layers of the Zhaojinggou Ta—Nb deposit contains 352 to 512 ppm Nb, 79 to 142 ppm Ta and 1428 to 2877 ppm Sn, values which are comparable with those of mica in the Yichun and Huangshan granite in China (Li et al., 2015; Zhu et al., 2018), and the Cínovec granite in the Czech Republic (Johan et al., 2012) (Fig. 8). This is probably because mica in the UST layers crystallized in an early magmatic stage prior to extensive crystallization of columbite.

Mica in the albite granite is commonly interstitial to albite laths and euhedral coarse-grained columbite (Fig. 5b). In a few cases, fine-grained, needle-like columbite is enclosed within mica (Fig. 5c). This indicates that the mica crystallized later than columbite, which is why mica in the granite has so much lower values of Nb, Ta, and Sn than mica in the UST layers (Fig. 8a–d). In addition, mica in the granite shows irregular zoning patterns in the BSE images (Fig. 4a,b); the bright

domains of F-rich zinnwaldite have high Li and Rb, but low Sn, W and Ba relative to the dark domains of F-poor muscovite (Fig. 9). This suggests that the F-rich zinnwaldite crystallized from highly evolved magma (Li et al., 2015). In contrast, the F-poor muscovite with high Al, Mn, Ba, Sn, and W concentrations may have crystallized from later hydrothermal fluids, which is consistent with the local abundance of muscovite in the apical parts of peraluminous granitic plutons (e.g., Breiter et al., 2019). The complex zoning patterns of mica in the granite indicate that the primary zinnwaldite was partially modified by later W, Sn, Ba, Mn and Al-rich hydrothermal fluids. Hydrothermal overprinting is also recorded in the REE patterns of the zircon (Fig. 11). The W-rich hydrothermal fluids may have migrated along faults to form the wolframite-quartz veins in the wall rocks (Fig. 2a). Mica in the greisen veins has a composition similar to that of muscovite in the granite (Figs. 7 and 8), suggesting that both were formed by hydrothermal processes.

9.4. Crystallization of the tantalite in the magmatic-hydrothermal transitional stage

Euhedral columbite grains (Fig. 5a) in the albite granite are magmatic in origin and crystallized due to the oversaturation of Nb and Ta in the peraluminous, granitic magmas (Linnen and Cuney, 2005). Tantalum concentrations in coarse-grained columbite crystals increase slightly from the center outwards (Fig. 5e,f), which is consistent with
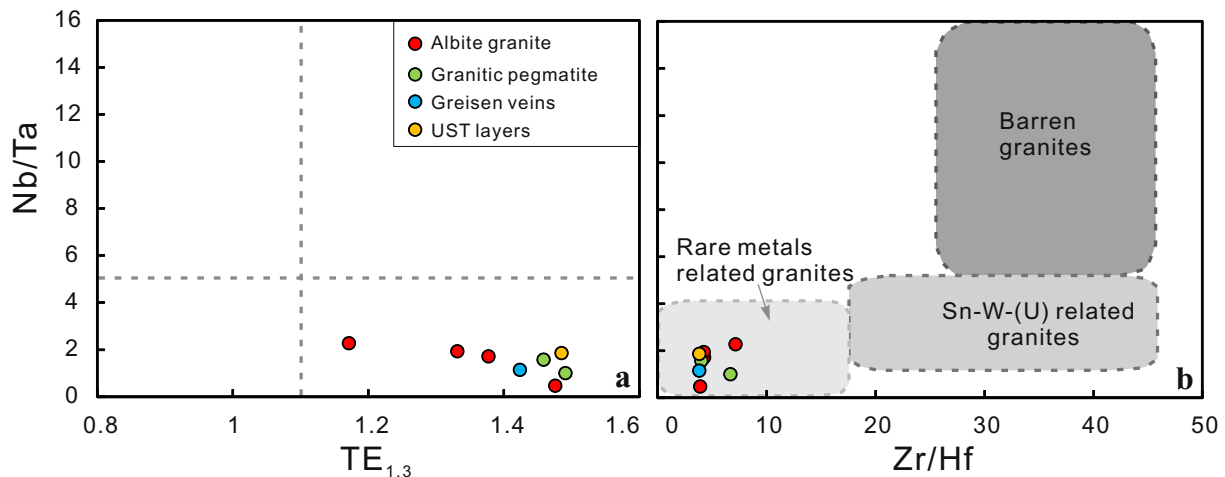

Fig. 14. Plots of Nb/Ta vs. TE$_{1,3}$ (a) and Nb/Ta vs. Zr/Hf (b) of rocks from the Zhaojinggou Ta—Nb deposit. The reference fields are from Ballouard et al. (2016).
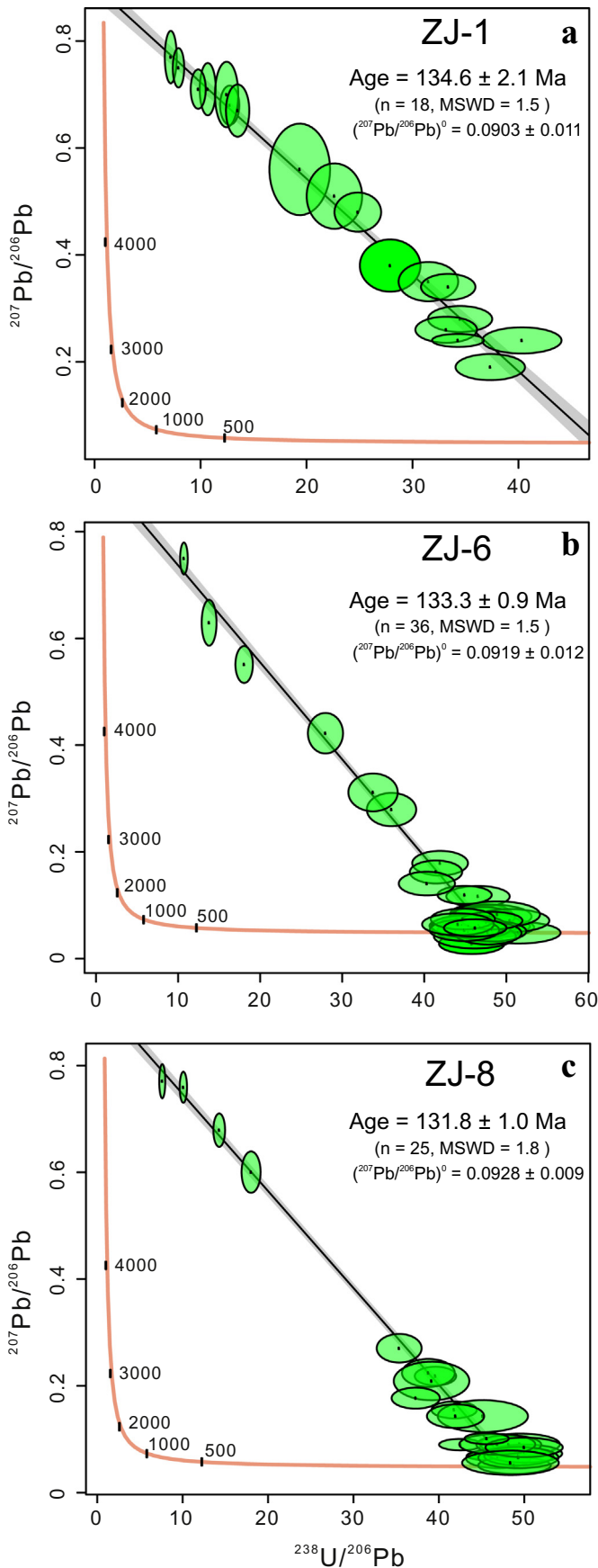
Fig. 15. Tera-Wasserburg U—Pb plots for the columbite.

a systematic decrease of Nb/Ta caused by the crystallization of columbite from silicate magma (Linnen et al., 2014).

Patches of tantalite may rim columbite grains or penetrate the grains along micro-cracks (Fig. 5e,i), indicating that the tantalite postdates the columbite. The patchy tantalite exhibits irregular disequilibrium boundaries with the euhedral columbite which still shows oscillatory zoning (Fig. 5g). In addition, the patchy tantalite contains much higher Ta concentrations than the euhedral columbite (Fig. 10a), and there is a compositional gap between the two. This suggests that the tantalite patches/rims were formed by replacement of columbite by a hydrosilicate melt in the magmatic-hydrothermal transitional stage (Wu et al., 2018). The hydrosilicate melt was enriched in Ta, F and Sn (Zhu et al., 2015) and other high field strength elements (HFSE, e.g. Zr) (Van Lichtervelde et al., 2007) as shown by the intergrowths of tantalite with cassiterite, zircon, and monazite (Figs. 5e,h,i and 6c,d,f). In some cases, the tantalite is enclosed within fluorite that is interstitial to albite (Fig. 5h). The F-rich hydrosilicate melt would have selectively concentrated REE, leading to the observed tetrad REE patterns (Fig. 13a) (Jahn et al., 2001; Veksler et al., 2005; Zhao et al., 1992; Zhao et al., 2002), which is consistent with the presence of abundant monazite and xenotime grains within the fluorite (Fig. 5g–i). Therefore, the tantalite patches/rims around columbite likely formed by dissolution of the columbite and precipitation from a Ta- and F-rich hydrosilicate melt in the magmatic-hydrothermal transitional stage.

10. Conclusions

The early Cretaceous Zhaojinggou Ta—Nb deposit is hosted in a peraluminous granite body that formed coincident with the peak stage of lithospheric thinning and destruction of the North China Craton, which could be a potential targeted exploration area for Ta mineralization in China. The columbite in the Zhaojinggou deposit crystallized from a highly evolved peraluminous granitic magma. The Ta enrichment in the columbite is attributed to replacement of the columbite by Ta- and F-rich hydrosilicate melt in the magmatic-hydrothermal transitional stage. Tungsten-rich hydrothermal fluids may have migrated into the country rocks where they formed wolframite-quartz veins around the granite body.

Declaration of Competing Interest

The authors declare that they have no known competing financial interests or personal relationships that could have appeared to influence the work reported in this paper.

Appendix A. Supplementary data

Supplementary data to this article can be found online at https://doi.org/10.1016/j.lithos.2020.105648.

References

Alfonso, P., Hamid, S.A., García-Vallès, M., Llorens, T., López, Moro F.J., Tomasa, O., Calvo, D., Guasch, E., Anticoi, H., Oliva, J., Parcerisa, D., Polonio, F., 2018. Textural and mineral-chemistry constraints on columbite-group minerals in the Penouta deposit: evidence from magmatic and fluid-related processes. Mineral. Mag. 82, 199–222.

Anderson, M.O., Lentz, D.R., McFarlane, C.R.M., Falck, H., 2013. Geological, geochemical and textural study of an LCT pegmatite: implications for the magmatic versus metasomatic origin of Nb-Ta mineralization in the Moose II pegmatite, Northwest Territories, Canada. J. Geosci. 58 (4), 299–320.

Ballouard, C., Poujol, M., Boulvais, P., Branquet, Y., Tartèse, R., Vigneresse, J.L., 2016. Nb-Ta fractionation in peraluminous granites: a marker of the magmatic-hydrothermal transition. Geology 44, 231–234.

Breiter, K., Hložková, M., Korbelová, Z., Galiová, M.V., 2019. Diversity of lithium mica compositions in mineralized granite–greisen system: Cínovec Li-Sn-W deposit, Erzgebirge. Ore Geol. Rev. 100, 12–27.

Černý, P., Ercit, T.S., Wise, M.A., 1992. The tantalite-tapiolite gap: natural assemblages versus experimental data. Can. Mineral. 30, 587–596.

Chai, H., Wu, J.L., 2013. The albite granite and mineralization of Zhaojinggou Nb-Ta deposit, Wuchuan County, Inner Mongolia. Inner Mongolia Sci. Technol. Econ. 15, 69–71 (in Chinese).

Che, X.D., Wu, F.Y., Wang, R.C., Gerdes, A., Ji, W.Q., Zhao, Z.H., Yang, J.H., Zhu, Z.Y., 2015. In situ U-Pb isotopic dating of columbite-tantalite by LA-ICP-MS. Ore Geol. Rev. 65, 979–989.

Davis, G.A., Darby, B.J., Yadong, Z., Spell, T.L., 2002. Geometric and temporal evolution of an extensional detachment fault, Hohhot metamorphic core complex, Inner Mongolia, China. Geology 30, 1003–1006.

Dostal, J., Kontak, D.J., Gerel, O., Shellnutt, J.G., Fayek, M., 2015. Cretaceous ongonites (topaz-bearing albite-rich microleucogranites) from Ongon Khairkhan, Central Mongolia: Products of extreme magmatic fractionation and pervasive metasomatic fluid: rock interaction. Lithos 236-237, 173–189.

Foster, M.D., 1960. Interpretation of the composition of lithium micas. US Geological Survey Professional Paper. 354, p. 147.

Gao, Y., Sun, Yan, Zhao, Z., Li, J.K., He, H.H., Yang, Y.Q., 2017. ^{40}Ar-^{39}Ar dating of muscovite from the zhaojinggou Nb-Ta polymetallic deposit in Wuchuan County of inner mongolia and its geological implications. Rock Min. Anal. 36 (5), 551–558 (in Chinese with English abstract).

Helba, H., Trumbull, R.B., Morteani, G., Khalil, S.O., Arslan, A., 1997. Geochemical and petrographic studies of Ta mineralization in the Nuweibi albite granite complex, Eastern Desert, Egypt. Mineral. Deposita 32, 164–179.

Hoskin, P.W.O., 2005. Trace-element composition of hydrothermal zircon and the alteration of Hadean zircon from the Jack Hills, Australia. Geochim. Cosmochim. Acta 69, 637–648.

Huang, X.L., Wang, R.C., Chen, X.M., Hu, H., Liu, C.S., 2002. Vertical variations in the mineralogy of the Yichun topaz-lepidolite granite, Jiangxi Province, southern China. Can. Mineral. 40 (4), 1047–1068.

Irber, W., 1999. The lanthanide tetrad effect and its correlation with K/Rb, Eu/Eu∗, Sr/Eu, Y/Ho, and Zr/Hf of evolving peraluminous granite suites. Geochim. Cosmochim. Acta 63, 489–508.

Jahn, B.M., Wu, F.Y., Capdevila, R., Martineau, F., Zhao, Z.H., Wang, Y.X., 2001. Highly evolved juvenile granites with tetrad REE patterns: the Woduhe and Baerzhe granites from the Great Xing'an Mountains in NE China. Lithos 59, 171–198.

Johan, Z., Strnad, L., Johan, V., 2012. Evolution of the Cínovec (Zinnwald) granite cupola: Czech Republic: composition of feldspars and micas, a clue to the origin of W, Sn mineralization. Can. Mineral. 50, 1131–1148.

Kaeter, D., Barros, R., Menuge, J.F., Chew, D.M., 2018. The magmatic–hydrothermal transition in rare-element pegmatites from Southeast Ireland: LA-ICP-MS chemical mapping of muscovite and columbite–tantalite. Geochim. Cosmochim. Acta 240, 98–130.

Li, J.W., Bi, S.J., Selby, D., Chen, L., Vasconcelos, P., Thiede, D., Zhou, M.F., Zhao, X.F., Li, Z.K., Qiu, H.N., 2012. Giant Mesozoic gold provinces related to the destruction of the North China craton. Earth Planet. Sci. Lett. 349–350, 26–37.

Li, J., Huang, X.L., He, P.L., Li, W.X., Yu, Y., Chen, L., 2015. In situ analyses of micas in the Yashan granite, South China: Constraints on magmatic and hydrothermal evolutions of W and Ta-Nb bearing granites. Ore Geol. Rev. 65, 793–810.

Li, Z.D., Li, X.G., Cui, Y.R., Li, G.Z., Zhang, J., Guo, H., Liu, W.G., Zhang, C., Yu, R.A., Xie, Y., Wang, J.Y., 2019. Yanshanian Mineralization of Zhaojinggou Nb-Ta Deposit InnerMongolia: Evidences from the Monaziteand Zircon LA-MC-ICP-MS U-Pb and Biotite ^{40}Ar-^{39}Ar Geochronology. Earth Sci. 44 (1), 234–247 (in Chinese with English abstract).

Liang, Q.L., Jiang, S.H., Liu, Y.F., 2013. Petrogenesis of the Donghouding A-type Granite in Northern Hebei: Constraints from Geochemistry, Zircon U-Pb Dating and Sr-Nd-Pb-Hf Isotopic Composition. Geol. Rev. 6, 1119–1130 (in Chinese with English abstract).

Linnen, R.L., Cuney, M., 2005. Granite-related rare-element deposits and experimental constraints on Ta-Nb-W-Sn-Zr-Hf mineralization. In: Linnen, R.L., Samson, I.M. (Eds.), Rare-Element Geochemistry and Mineral Deposits. GAC Short Course Notes. 17, pp. 45–67.

Linnen, R.L., Keppler, H., 1997. Columbite solubility in granitic melts: consequences for the enrichment and fractionation of Nb and Ta in the Earth's crust. Contrib. Mineral. Petrol. 128, 213–227.

Linnen, R.L., Samson, I.M., Williams-Jones, A.E., Chakhmouradian, A.R., 2014. Geochemistry of the rare-earth element, Nb, Ta, Hf, and Zr deposits. In: Heinrich, H., Karl, T. (Eds.), Reference Module in Earth Systems and Environmental Sciences Treatise on Geochemistry. Elsevier Science, pp. 543–564.

Liu, J., Davis, G.A., Lin, Z., Wu, F., 2005. The Liaonan metamorphic core complex, Southeastern Liaoning Province, North China: a likely contributor to cretaceous rotation of Eastern Liaoning, Korea and contiguous areas. Tectonophysics 407, 65–80.

Liu, Y., Jiang, S.H., Chen, C.L., 2015. Petrogenesis of the Jiashan Syenite in Chengde, Hebei Province Geochemical and Sr-Nd-Pb-Hf Isotopic evidence. Acta Petrol. Mineral. 34, 14–34 (in Chinese with English abstract).

London, 2009. The origin of primary textures in granitic pegmatites. Can. Mineral. 47, 697–724.

Monier, G., Robert, J.L., 1986. Evolution of the miscibility gap between muscovite and biotite solid solutions with increasing lithium content: an experimental study in the system K$_2$O-Li$_2$O-MgO-FeO-Al$_2$O$_3$-SiO$_2$-H$_2$O-HF at 600°C, 2 kbar P_{H2O}: comparison with natural lithium micas. Mineral. Mag. 50, 641–651.

Neiva, A.M.R., Gomes, M.E.P., Silva, P.B., 2015. Two generations of zoned crystals of columbite-group minerals from granitic aplite-pegmatite in the Gouveia area, Central Portugal. Eur. J. Mineral. 27 771–482.

Nie, F.J., Wang, F.X., Zhao, Y.A., Sun, Y., Chai, H., 2013. Geological features and origin of Zhaojinggou Nb-Ta deposit in Wuchuan county，Inner Mongolia. Mineral Deposits 32 (4), 730–743 (in Chinese with English abstract).

Partington, G.A., McNaughton, N.J., Williams, I.S., 1995. A review of the geology, mineralization, and geochronology of the Greenbushes Pegmatite, Western Australia. Econ. Geol. 90, 616–635.

Pollard, P.J., 1986. Geochemistry of granites associated with Tantalum and Niobium mineralization. In: Möller, P., Cerny, P., Saupé, F. (Eds.), Lanthanides, Tantalum and Niobium: Mineralogy, Geochemistry, Characteristics of Primary Ore Deposits. Springer-Verlag, Berlin, pp. 145–168.

Rao, C., Wang, R.C., Hu, H., Zhang, W.L., 2009. Complex internal textures in oxide minerals from the Nanping No. 31 dyke of granitic pegmatite, Fujian Province, southeastern China. Can. Mineral. 47, 1195–1212.

Ren, J., Tamaki, K., Li, S., Junxia, Z., 2002. Late Mesozoic and Cenozoic rifting and its dynamic setting in Eastern China and adjacent areas. Tectonophysics 344, 175–205.

Reyf, F.G., Seltmann, R., Zaraisky, G.P., 2000. The role of magmatic processes in the formation of banded Li-Fi-enriched granites from the Orlovka Tantalum deposit, Transbaikalia, Russia: Microthermomeric evidence. Can. Mineral. 38, 915–936.

Shannon, J.R., Walker, B.M., Carten, R.B., Geraghty, E.P., 1982. Unidirectional solidification textures and their significance in determining relative ages of intrusions at the Henderson Mine, Colorado. Geology 10, 293–297.

Sun, S.S., McDonough, W.F., 1989. Chemical and isotopic systematics of oceanic basalt: implications for mantle composition and processes. Geol. Soc. Lond. Spec. Publ. 42, 313–345.

Tindle, A.G., Breaks, F.W., 2000. Columbite-tantalite mineral chemistry from rare-element granitic pegmatites: Separation Lakeh area, N.W. Ontario, Canada. Mineral. Petrol. 70, 165–198.

Tindle, A.G., Webb, P.C., 1990. Estimation of lithium contents in trioctahedral micas using microprobe data: application tomicas fromgranitic rocks. Eur. J. Mineral. 2, 595–610.

Van Lichtervelde, M., Linnen, R.L., Salvi, S., Didier, B., 2007. Textures and chemical evolutions in tantalum oxides: a discussion of magmatic versus metasomatic origins for Ta mineralization in the Tanco lower Pegmatite, Manitoba, Canada. Econ. Geol. 102, 257–276.

Veksler, I.V., Dorfman, A.M., Kamenetsky, M., Dulski, P., Dingwell, D.B., 2005. Partitioning of lanthanides and Y between immiscible silicate and fluoride melts, fluorine and cryolite and the origin of the lanthanide tetrad effect in igneous rocks. Geochim. Cosmochim. Acta 69, 2847–2868.

Vermeesch, P., 2018. IsoplotR: a free and open toolbox for geochronology. Geosci. Front. 9, 1479–1493.

Wang, R.C., Francois, F., Xu, S.J., Chen, X.M., Monchoux, P., 1997. The association of columbite, tantalite and tapiolite in the Suzhou granite, China. Can. Mineral. 35, 699–706.

Wang, F.Y., Ge, C., Ning, S.Y., Nie, L.Q., Zhong, G.X., White, N.C., 2017. A new approach to LA-ICP-MS mapping and application in geology. Acta Petrol. Sin. 33, 3422–3436.

Wu, F.Y., Lin, J.Q., Wilde, S.A., Zhang, X.O., Yang, J.H., 2005. Nature and significance of the early cretaceous giant igneous event in eastern China. Earth Planet. Sci. Lett. 233, 103–119.

Wu, M.Q., Samson, I.M., Zhang, D.H., 2018. Textural features and chemical evolution in Ta-Nb Oxides: implications for deuteric rare-metal mineralization in the yichun granite-marginal pegmatite, Southeastern China. Econ. Geol. 113, 937–960.

Xu, Y.G., 2001. Thermo-tectonic destruction of the archaean lithospheric keel beneath the sino-korean craton in China: evidence, timing and mechanism. Phys. Chem. Earth Solid Earth Geod. 26, 747–757.

Yang, J.H., Wu, F.Y., Wilde, S.A., Chen, F., Liu, X.M., Xie, L.W., 2008. Petrogenesis of an Alkali Syenite–Granite–Rhyolite Suite in the YANSHAN FOLD AND THRUST BElt, Eastern North China Craton: geochronological, geochemical and Nd-Sr-Hf isotopic evidence for lithospheric thinning. J. Petrol. 49, 315–351.

Yang, W.B., Niu, H.C., Shan, Q., Sun, W.D., Zhang, H., Li, N.B., Jiang, Y.H., Yu, X.Y., 2014. Geochemistry of magmatic and hydrothermal zircon from the highly evolved Baerzhe alkaline granite: implications for Zr-REE-Nb mineralization. Mineral. Deposita 49, 451–470.

Ye, D.L., Ren, Y.X., Tai, D.Q., 1991. The study on the characteristics of geochemistry and mineralization of the M111 rare metal contained granitic intrusion in Xinglong, Heibei. Geoscience 5, 13–23 (in Chinese with English abstract).

Zeng, L.J., 2016. Petrogenesis and Magmatic-Hydrothermal Evolution of A-Type Granite in the Yanshan and Kuiqi Areas. Ph.D.thesis. University of Chinese Academy of Sciences, Beijing.

Zhai, M.G., Santosh, M., 2011. The early Precambrian odyssey of the North China Craton: a synoptic overview. Gondwana Res. 20, 6–25.

Zhao, Z.H., Akimasa, M., Shabani, M.B., 1992. Tetrad effects of rare-earth elements in rare-metal granites. Geochimica 3, 221–233 (in Chinese with English abstract).

Zhao, G.C., Wilde, S.A., Cawood, P.A., Sun, M., 2001. Archean blocks and their boundaries in the North China craton: lithological, geochemical, structural and p-t path constraints and tectonic evolution. Precambrian Res. 107 (1), 45–73.

Zhao, Z.H., Xiong, X.L., Han, X.D., Wang, Y.X., Wang, Q., Bao, Z.W., Jahn, B.M., 2002. Controls on the REE tetrad effect in granites: evidence from the Qianlishan and Baerzhe Granites, China. Geochem. J. 36, 527–543.

Zhao, G.C., Sun, M., Wilde, S.A., Li, Z., 2005. Late Archean to Paleoproterozoic evolution of the North China Craton: key issues revisited. Precambrian Res. 136 (2), 177–202.

Zhu, R.X., Yang, J.H., Wu, F.Y., 2012. Timing of destruction of the North China Craton. Lithos 149, 51–60.

Zhu, Z.Y., Wang, R.C., Che, X.D., Zhu, J.C., Wei, X.L., Huang, X., 2015. Magmatic-hydrothermal rare element mineralization in the Songshugang granite (northeastern Jiangxi, China): Insights from an electron-microprobe study of Nb-Ta-Zr minerals. Ore Geol. Rev. 65, 749–760.

Zhu, Z.Y., Wang, R.C., Marignac, C., Cuney, M., Mercadier, J., Che, X.D., Lespinasse, M., 2018. A new style of rare metal granite with Nb-rich mica: the early cretaceous Huangshan rare-metal granite suite, Northeast Jiangxi Province, Southeast China. Am. Mineral. 103 (10), 1530–1544.